ELSEVIER

International Journal of Refractory Metals & Hard Materials 18 (2000) 307–322

International Journal of
REFRACTORY METALS
& HARD MATERIALS

Fundamentals of liquid phase sintering for modern cermets and functionally graded cemented carbonitrides (FGCC)

Limin Chen [a,*], Walter Lengauer [b], Peter Ettmayer [b], Klaus Dreyer [c], Hans W. Daub [c], Dieter Kassel [c]

[a] *Austrian Research Center, Division of Materials Technology, A-2444, Austria*
[b] *Institute for Chemical Technology of Inorganic Materials, Vienna University of Technology, Getreidemarkt 9/161, A-1060, Austria*
[c] *WIDIA GmbH, Munchener Str. 90, D-45145 Essen, Germany*

Received 9 May 2000

Abstract

Metallurgical reactions and microstructure developments during sintering of modern cermets and functionally graded cemented carbonitrides (FGCC) were investigated by modern analytical methods such as mass spectrometer (MS), differential thermal analysis (DTA), differential scanning calorimeter (DSC), dilatometer (DIL), microscopy and analytical electronic microscopy with energy dispersive spectrometer (EDS). The complex phase reactions and phase equilibria in the multi-component system Ti/Mo/W/Ta/Nb/C,N-Co/Ni were studied. The melting behavior models in the systems of TiC–WC/MoC–Ni/Co, TiC–TiN–WC–Co and TiCN–TaC–WC–Co have been established. By an in-depth understanding of the mechanisms that govern the sintering processing and metallurgical reactions, new cermets and different types of FGCC with desired microstructures and properties were developed.

Keywords: Functionally graded cemented carbonitrides; Cermets; Cutting tools; Phase diagram; Thermal analysis

1. Introduction

The importance of introducing nitrogen in the form of TiN into TiC–Ni/Mo cermets was discovered by Kieffer et al. around 1970 [1]. Systematic researches afterwards led to a new generation of modern cutting cermets, which are characterized by multi-components with TiC and TiN, or alternatively, TiCN as the basic ingredients. Additions of Mo_2C, WC, TaC, NbC and VC add up to 20–40 mass% of the total. The binder alloys usually contain Ni and Co of the order of 10–15 mass% but in varying relative amounts. The performance of the modern cutting cermets can match or even be better than that of coated cemented carbides. Some excellent reviews on the modern cermets are given in the literature [2–5].

As for the coated cemented carbides, the surface zone of the "state-of-the-art" substrate often features a Co-enriched and cubic-phase free layer (CFL). During interrupted machining, such a CFL layer underneath the ceramic coatings absorbs most of the energy so that the impact resistance of the coated carbide grades is greatly improved. The CFL surface layer is usually prepared by a post-sintering treatment of nitrogen-containing alloys under (high) vacuum at cooling speeds less than 10 K/min. [6–10]. The denitridation (i.e., decomposition of nitrides or carbonitrides) caused by vacuum treatment is believed to form the CFL character on the surface of the substrates.

The surface zone can also be modified into an unique structure with a gradation enriched in TiCN cubic phase and depleted in WC and Co/Ni binder. So-called functionally graded material (FGM) cemented carbonitrides are sintered in a nitrogen-containing atmosphere. Inserts with as-sintered single or multi-FGM layers have been developed and were reported to perform better than the coated carbides [11–16]. In addition to the improvement in the cutting performance, very costly coating process may be eliminated by the newly developed FGM technology. Saving potential is promising since coating process accounts for more than 15% of the total

* Corresponding author. Present address: SinterMet, Inc., West Hills Industrial Park, North Park Drive, Kittanning, PA 16201-8883, USA. Tel.: +1-724-548-7631; fax: +1-724-545-1824.
E-mail address: limin.chen@sintermet.com (L. Chen).

0263-4368/01/$ - see front matter
PII: S0263-4368(00)00041-X

manufacturing costs while sintering process accounts for only 5% [17].

Nitrogen plays a more and more critical role to develop new generation of cutting tool materials. However, with the addition of nitrogen (through carbonitrides, nitrides or nitrogen gas), the metallurgical reactions during sintering become much more complex and the sintering atmosphere has to be more accurately controlled [12–16,18,19]. The cutting tool industry is still lacking in understanding the mechanisms of liquid phase sintering of nitrogen-containing cemented carbides. The present work approaches to carry out a systematic research in order to fill in this gap.

2. Experimental procedures

2.1. Differential thermal analysis (DTA)

DTA was used to measure the melting point temperatures of experimental alloys with 33 wt% binder metal content or higher. Highly pure re-crystallized alumina and a platinum alloy were used as crucible and reference standard, respectively. The temperature was measured with a Pt/Rh thermocouple and the accuracy of the temperature measurement is estimated to be within ±3°C by the temperature calibration against known melting points of high purity Cu and Cu–Ni alloys.

2.2. Differential scanning calorimeter (DSC) measurements

The melting point temperatures of some industrial alloys were measured by a DSC system (Netzsch DSC 404). This system monitors the ΔT signal representing the difference in temperature between a sample and an inert reference material as a function of the temperature. The temperature was calibrated against the melting point of Au and the measurement error was within ±1°C.

2.3. Dilatometer (DIL) measurements

The shrinkage behaviors of the industrial alloys were monitored by a dilatometer (Netzsch DIL 402C, max. temperature 1600°C). The samples were heated under dynamic vacuum of $4–6 \times 10^{-4}$ mbar till 1300°C. Then the vacuum pump was then turned off and the samples were continually heated to 1500°C. The gas pressure rose to a few mbar during sintering.

2.4. Gas analysis by a mass spectrometer (MS)

Gases CO and N_2 released during sintering were monitored by a system illustrated in Fig. 1. In the MF furnace a high-pressure interface was inserted between the recipient and the quadrupole mass spectrometer system in order to be able to characterize the sintering atmosphere at pressures in the mbar ranges. This is necessary because a He gas stream has to be used to elute the gases from the crucible into the MS system. A gas flow system together with a second pump was used in order to sustain a constant pressure of 20 mbar. The ion fluxes of CO^+, N_2^+ and N^+ were recorded, calibrated against standard gas mixtures and introduced in a system of linear equations (because of the coincidence of N_2^+ and CO^+ at mass 28) for the CO and N_2 concentrations.

2.5. Solid–liquid reactions

"Solid compact–liquid metal" reaction couples were studied by embedding a piece of hot-pressed carbide

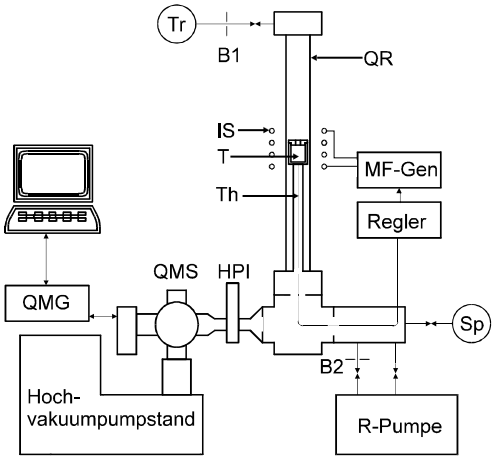

QMS	quadrupole mass spectrometer
QMG	QMS electronics
HPI	high pressure interface
Regler	temperature controller
MF-Gen	MF generator
IS	induction coil
T	crucible with sample
B1	orifice 1
B2	orifice 2
Tr	elution gas (He)
Sp	flushing gas
R-Pumpe	rotation pump
QR	silica tube
Th	thermo-element

Fig. 1. Schematic illustration of MS gas analysis system.

plate and Co or Ni powders in an alumina crucible. The reaction couples were heated up to 1550°C within 40 min in a BALZERS VSG 02 furnace equipped with a tungsten heating element under Ar atmosphere of 300 mbar. The electrical power of the device was turned off as soon as the samples had reached the vertex temperature of 1550°C. The specimens were then furnace cooled.

2.6. Microstructure evaluation

Microstructures were investigated by optical microscope, scanning electron microscope (SEM, model JEOL JSM 6400) and scanning transmission electron microscope (STEM, model H-800). Quantitative compositional analysis was performed by energy dispersive spectroscopy (EDS) detectors attached to SEM and STEM.

3. Results and discussion

3.1. Melting point temperatures measured by DTA

The onset points of DTA heating curves were used as melting point temperatures. The melting points of binary eutectic reactions: melts $\Rightarrow$ Co (or Ni) + (Ti, W)C (or (Ti, Mo)C) were measured by DTA using experimental alloys with 90 mol% binder metals. The results are given in Fig. 2. Due to the high binder content, all alloy components dissolved in the liquid melt at a maximum measurement temperature of about 1500°C. The addition of "MoC" does not change the melting points of TiC–Ni alloys, but decreases the melting points of TiC–Co alloys (see Figs. 2(a) and (c)). If WC is added, the melting points of TiC–Ni alloys will continuously increase from 1295°C to 1370°C (see Fig. 2(b)). A maximum melting point temperature was observed for the TiC–WC–Co alloys (see Fig. 2(d)).

Hundreds of nitrogen-containing alloys of WC–TiC–TiN–TaC-33 wt% Co were measured by DTA. The results are summarized in Figs. 2(e) and (f). Some alloys were observed by the SEM. As shown in Figs. 2(e) and (f), there exists a boundary line which divides the phase diagrams into two areas. The melting point temperatures were observed to be the same at 1350°C for all alloys located in the WC phase existing region, i.e., in the WC + (Ti,W)(C,N) + Co three-phase region (see Fig. 2(e)). In the (Ti,W)(C,N) + Co two-phase region, the melting point temperatures vary from 1350°C in terms of high TiC-containing alloys to 1450°C in terms of high TiN-containing alloys. The addition of TaC to the WC–TiCN–Co alloys decreases the solid solution of WC in (Ti,W,Ta)(C,N) cubic phase, yet does not influence the melting point temperatures (see Fig. 2(f)).

3.2. Melting behaviors of some industrial alloys measured by DSC

Industrial alloys contain much less amount of binder phase than the DTA experimental alloys. DSC was employed in order to measure the melting points of the industrial alloys accurately. Some DSC results are shown in Table 1 and Fig. 3.

DSC results coincide with the DTA results very well. The compositions of alloys #45, #32, #35 and #37 are located in the three-phase region of WC + (Ti,W)(C,N) + Co (see Figs. 2(e) and (f)). Regardless of their C/N and Ti/W ratios, these alloys have almost the same melting point temperature of about 1350°C (see Fig. 3). Comparing alloy #62 with alloy #45, alloy #62 has two onset point temperatures because it contains Co/Ni as binder instead of pure Co binder. Moreover, its melting temperature range (1338–1395°C) is broader than that of the alloy #45 (1347–1365°C). As shown in Figs. 2(b) and (d), WC–Co alloy has a lower quasi-binary eutectic temperature (1320°C) than WC–Ni alloy (1370°C). During heating of the alloy #62, WC reacts with Co at low temperature to form a liquid phase which is reflected by the first onset point on the DSC curve. The second onset point temperature of 1382°C reflects the second reaction: WC + Ni $\Rightarrow$ melt. Since cermet alloy #44 also has a mixed Co/Ni binder, it displays the same melting behavior as alloy #62. However, the first onset point temperature was not observed for the alloy #44 due to its much lower binder content compared to the alloy #62.

Cermet alloys #42 and #43 are located in the two-phase region of (Ti,W)(C,N) + Co (see Fig. 2(e)). Their onset point temperatures of 1416°C and 1410°C, respectively, are in good consistence with the corresponding DTA experimental alloys located in the same region. However, as TiN-cermet alloy #43 contains a hard phase composition of 90 mol% TiN and 10 mol% WC, its onset and peak point temperatures of cooling phase are significantly different from those of the heating phase (see Fig. 3 and Table 1). Moreover, the strength of the DSC peak of alloy #43 during cooling phase is much weaker than that during heating phase. Because denitridation was severe during heating phase for this very high nitrogen-containing alloy, η was formed during cooling. The formation of η phase consumes the liquid binder phase, which results in different onset and peak point temperatures as well as weak peak strength.

3.3. Shrinkage behaviors of some industrial alloys measured by DIL

Industrial cermet and cemented carbide alloys are usually sintered in the presence of liquid phase. The

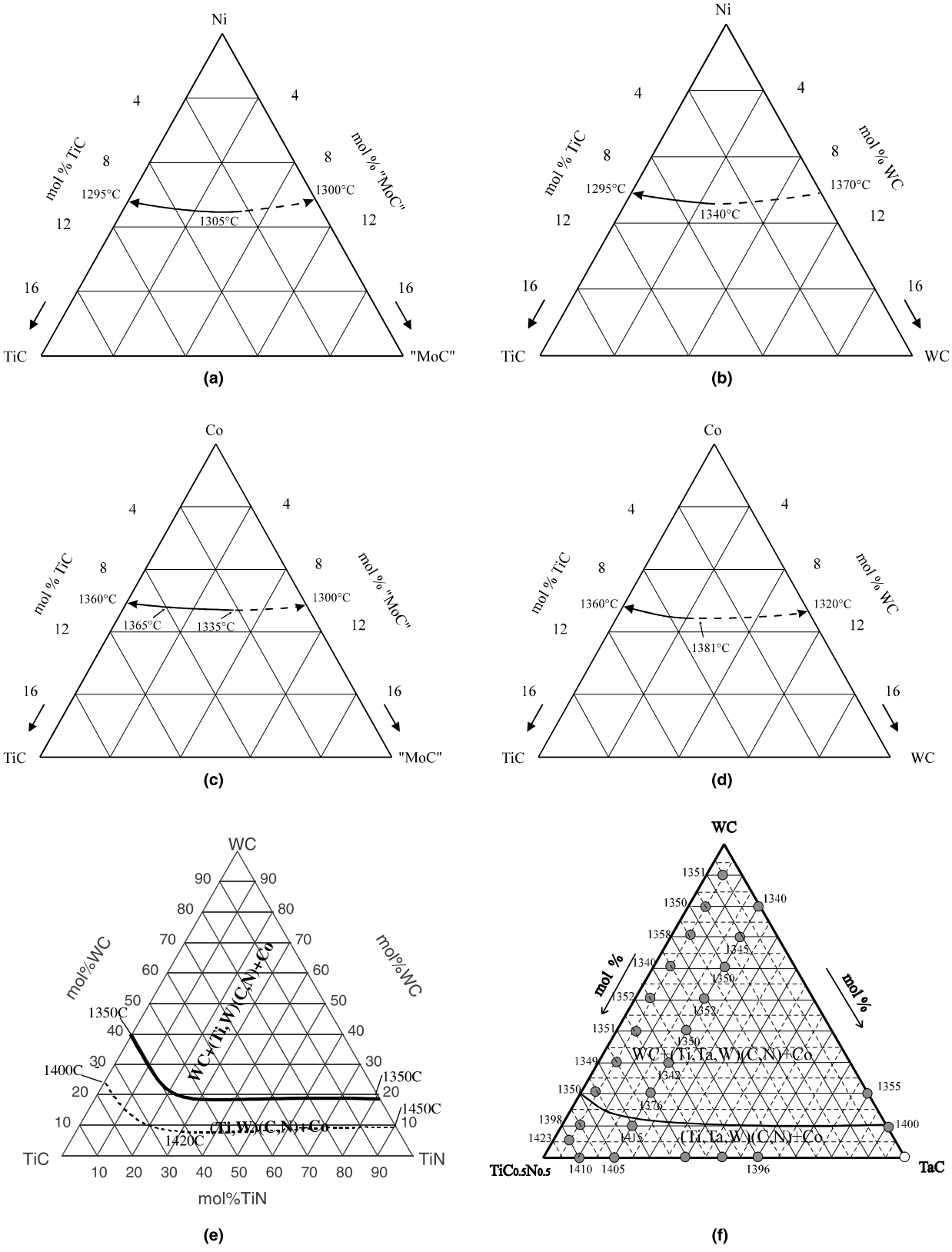

Fig. 2. Melting point temperatures measured by DTA.

Table 1
Onset and peak point temperatures of some industrial alloys measured by DSC

Alloys	Heating phase (°C)		Cooling phase (°C)		Phase observed	Remarks
	Onset	Peak	Onset	Peak		
#45	1347	1365	1355	1347	WC, Co	Cemented carbide
#62	1338/1382	1395	1391	1385	WC, Co/Ni	Cemented carbide
#32	1356	1367	1355	1347	WC, (Ti,W)C, Co	Cemented carbide
#35	1356	1367	1355	1344	WC, (Ti,W)(C,N), Co	Cemented carbonitride
#37	1358	1367	1351	1343	WC, TiN, Co	Cemented carbonitride
#44	1389	1404	1396	1383	WC, (Ti,W)(C,N), Co/Ni	TiCN cermet
#42	1416	1426	1414	1404	(Ti,W)(C,N), Co/Ni	TiCN cermet
#43	1410	1423	1370	1355	(Ti,W)(N,C), Co/Ni	TiN cermet

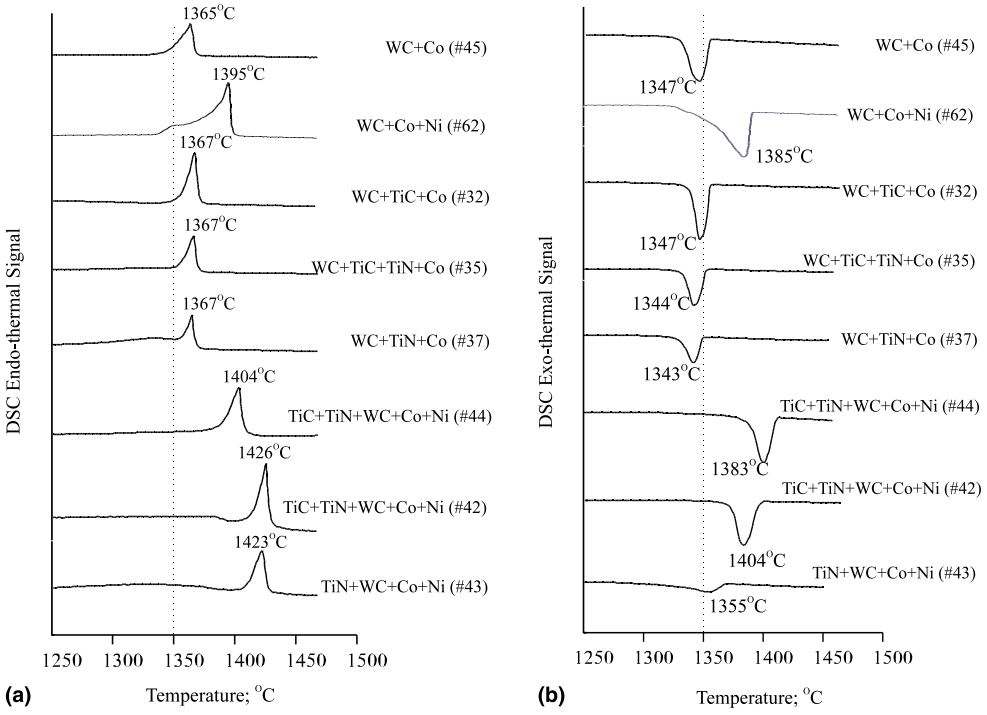

Fig. 3. DSC curves of some industrial alloys: (a) heating phase and (b) cooling phase.

liquid phase sintering mechanism features three stages: (1) particle re-arrangement, (2) formation of liquid phase and (3) final densification. Corresponding to the three stages of liquid phase sintering, three peaks on the DIL $\mathrm{d}L/(L_0\,\mathrm{d}t)\%/\mathrm{min}$ curve were observed as shown in Fig. 4. The corresponding peak temperatures are listed in Table 2. Samples shrink drastically when particle re-arrangement is detected by DIL. In the second sintering stage when liquid phase appears, shrinkage is almost completed as indicated by the DIL. In the final stage of the liquid phase sintering, almost all porosity is removed from the sintered body and full densification is reached. Depending on the alloy composition, maximum sintering temperature and other sintering parameters, microporosity may be residual in the sintered products.

All alloys have almost the same turning point temperature of about 1300°C for the first peak. As for the second peak, alloys #45, #32 and #35 have the same turning point temperature of about 1350°C. The second peak temperature for alloy #44 is 1400°C. The cermet alloys #42 and #43 have the highest second peak turning point temperature of about 1430°C. With increasing Ti and nitrogen (N) contents, the third peak becomes more significant in the order of alloys #35, #44, #42 and #44. However, the third peak was not evident with respect to the nitrogen-free alloys #45 and #32.

Therefore, the sintering temperature for industrial alloys should be at least higher than the second peak turning temperature in order to obtain fully densified products. According to the DIL measurements, the

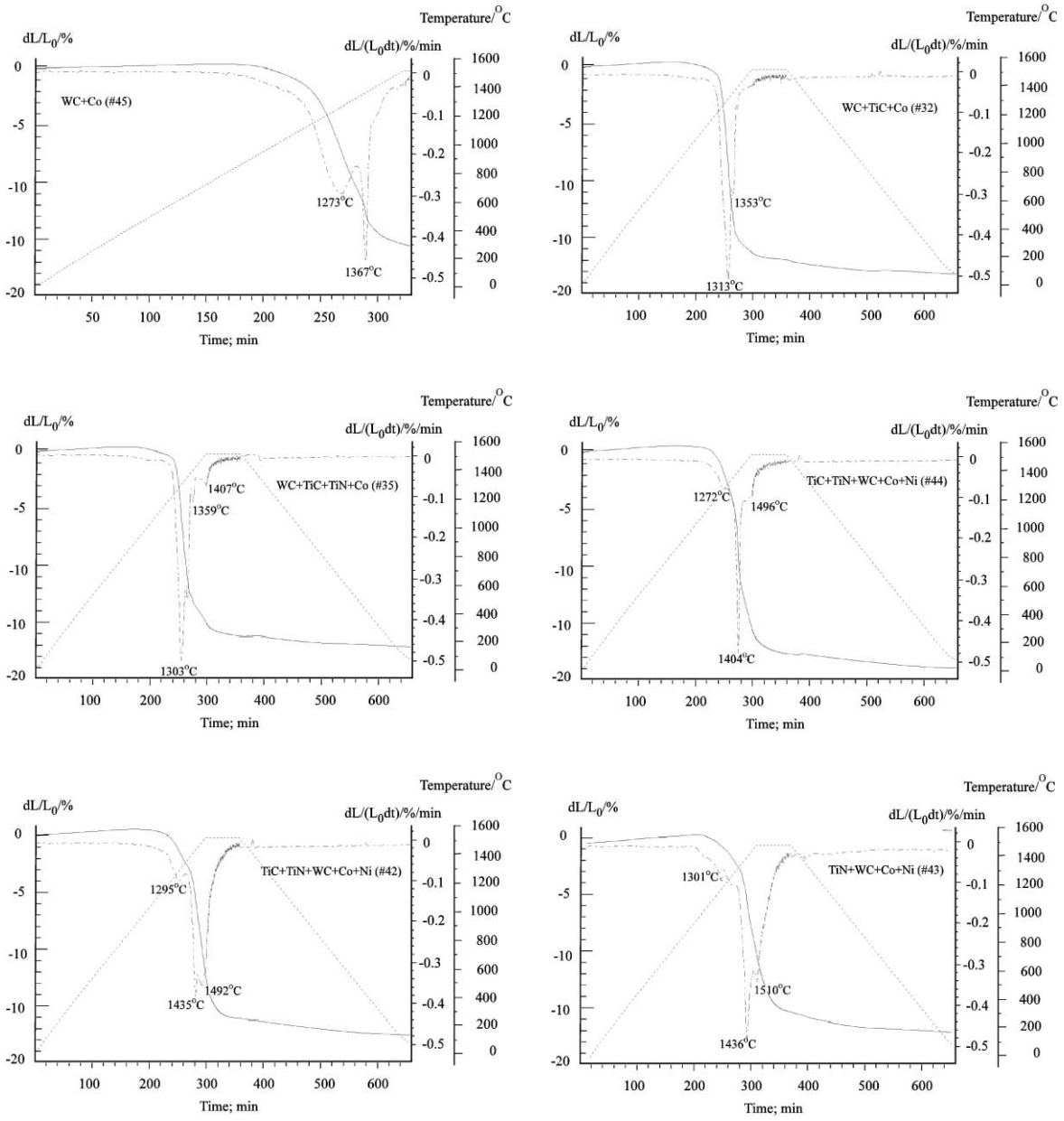

Fig. 4. Shrinkage behaviors of some industrial alloys measured by DIL.

Table 2
Turning point temperatures of some industrial alloys measured by DIL

Alloys	$dL/(L_0\,dt)\%/$ min curve (°C)			Phase observed	Remarks
	1st peak	2nd peak	3rd peak		
#45	1273	1367	–	WC, Co	Cemented carbide
#32	1313	1353	–	WC, (Ti,W)C, Co	Cemented carbide
#35	1303	1359	1407	WC, (Ti,W)(C,N), Co	Cemented carbonitride
#44	1272	1404	1496	WC, (Ti,W)(C,N), Co/Ni	TiCN cermet
#42	1295	1435	1492	(Ti,W)(C,N), Co/Ni	TiCN cermet
#43	1301	1436	1510	(Ti,W)(N,C), Co/Ni	TiN cermet

optimum sintering temperature will be about 1350–1400°C and 1450–1500°C for WC-based cemented carbides (or cemented carbonitrides) and TiCN-based modern cermets, respectively.

Comparing DSC with DIL measurements, the particle re-arrangement takes places before the formation of liquid phase. The second peak of DIL curves (second stage of the liquid phase sintering) is observed as soon as the liquid phase is detected by DSC (see Tables 1and 2, Figs. 3 and 4).

3.4. Gas evolution during sintering

As shown in Fig. 5(a), the oxide film on the surface of Co particles is removed below 500°C. Three CO peaks were observed for either pure WC or TiC powders due to the fact that WO_3 and TiO_2 oxides are reduced through three steps: $WO_3 \Rightarrow W_4O_{11} \Rightarrow WO_2 \Rightarrow W$ and $TiO_2 \Rightarrow Ti_2O_3 \Rightarrow TiO \Rightarrow Ti$, respectively. Pure TiN powder is very stable against vacuum up to 1500°C. The gas evolution of WC + TiC powder mixture combines those features of separate WC and TiC powders. However, only two main CO peaks were observed for the WC + TiC powder mixture. Probably, reduction of oxides is easier for the WC + TiC powder mixture than for the signal WC or TiC powders. As for the WC + TiN powder mixture, CO and N_2 peaks were observed at temperatures above 1400°C. Reaction between WC and TiN must happen to release N_2. This is due to the thermodynamic instability of TiN in the presence of WC or other carbon source (see Section 3.5).

The gas evolution of some industrial alloys is given in Fig. 5(b). For WC + Co alloy #45, the outgassing process is almost completed at a temperature around 1000°C. Compared to WC + TiC powder mixture, alloy #32 (WC + TiC + Co) shows lower temperatures of CO outgassing. The effect of Co binder on the mechanism of gas evolution has also been observed in other TiC and/or TiN-containing alloys as shown in Fig. 5. N_2 peak was not observed in the pure WC + TiN powder mixture below 1400°C. However, in the presence of Co and/or Ni binder metals, N_2 starts to release at a temperature of about 1200°C for all TiN-containing alloys #35, #37 and #42. The gas evolution terminates at about 1300°C for all TiC/TiN-containing alloys.

During sintering of cermets or cemented carbonitrides, the evolution of CO from chemisorbed or chemically bonded oxygen on the surface of the powder particles features a few stages at different temperatures around 500°C, 650°C and 1000°C. The different outgassing temperatures correspond to the reductions of different oxides existing on the surface of the powder particles. The main CO peak appears around 1100–1200°C and fades out at about 1250°C. The presence of Co/Ni binder greatly accelerates the elution of CO and therefore improves the removal of the oxide layers from the powder particles. However, denitridation is accelerated by the presence of Co/Ni binder too. The elution of nitrogen sets in at about 1200°C and has a very marked maximum at about 1300°C. With the onset of particle re-arrangement at approximately 1300°C, CO and nitrogen elution falls drastically

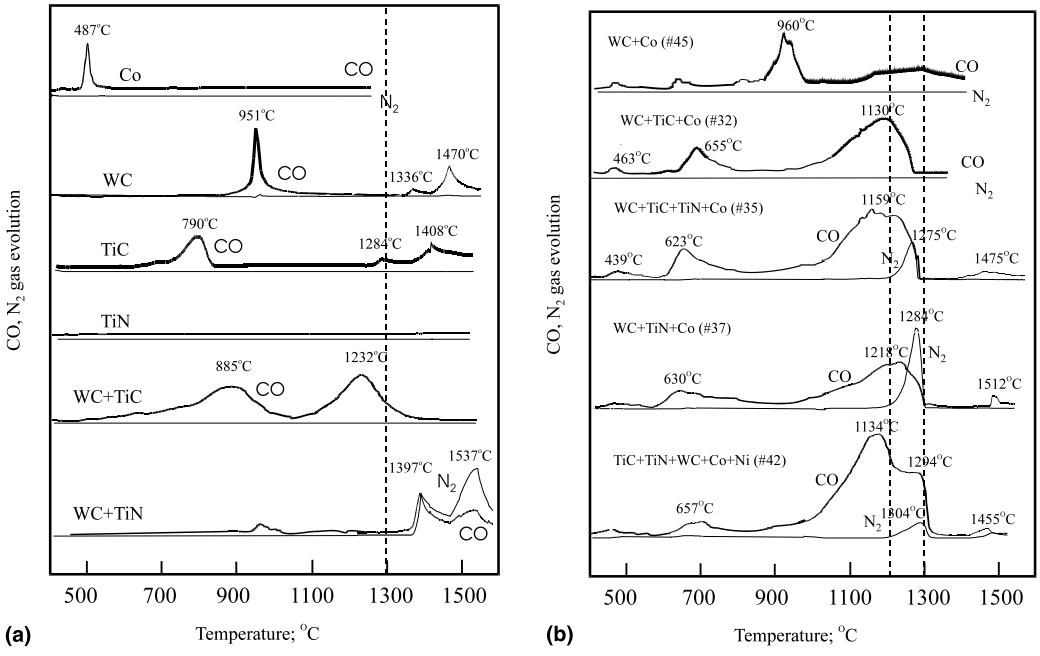

Fig. 5. Gas evolution measured by MS during heating of: (a) Co, WC, TiC, TiN, WC + TiC and WC + TiN powders; (b) some industrial alloys.

because of the very strong shrinkage of the compacts. With increasing temperature, the rate of CO and nitrogen elution begin to gradually increase again but only around at 1500°C. The formation of liquid phase is not influenced by the starting materials of either pre-alloyed quaternary carbonitrides or powder mixtures of single TiC, TiN and WC. In the scope of our experiments, even the stoichiometric factor x of the hard phase (Ti,W)(C,N)$_x$ ($x = 0.85 - 1$) does not affect the melting point temperatures very much.

3.5. Thermodynamic stability of hard phases

The thermodynamic stability of TiC–TiN–WC carbonitrides was studied by X-ray diffractometer (XRD) and the experimental details are given in [13,14]. As shown in Fig. 6, two fcc (Ti,W)(C,N) phases δ_1 and/or δ_2, where $\delta_1 - (\mathrm{Ti}_x, \mathrm{W}_{1-x})(\mathrm{C}_{x'}, \mathrm{N}_{1-x'})$ is rich in Ti and N, and $\delta_2 - (\mathrm{Ti}_y, \mathrm{W}_{1-y})(\mathrm{C}_{y'}, \mathrm{N}_{1-y'})$ is rich in W and C, were observed in the whole compositional range of the WC–TiC–TiN hard phase system. Since the compositions of the two fcc phases were quite similar, profile fitting with the Difpatan X-ray diffraction program had to be applied to identify the phases. In the compositional region A, only one fcc (Ti,W)(C,N) phase was observed. Two fcc phases δ_1 and δ_2 were observed in the compositional region B. In the compositional regions C, D and E, hex-WC, bcc-W and hex-W_2C, respectively, coexisted with δ_1 and δ_2.

The TiC–TiN–MoC system can be treated as a reciprocal system: $\mathrm{TiC} + \mathrm{MoN} \Longleftrightarrow \mathrm{TiN} + \mathrm{MoC}$ according to Rudy [19]. Of particular interest in this system are the phase equilibria within the range of the solid solution $(\mathrm{Ti}, \mathrm{Mo})(\mathrm{C}, \mathrm{N})_z (0.8 < z < 1)$, where, depending upon temperature and composition, a miscibility gap exists featuring two iso-structural phases: α' – a molybdenum poor and nitrogen-rich (Ti,Mo)(C,N) phase, and α'' – a molybdenum-rich and nitrogen poor (Ti,Mo)(C,N) phase. The separation of these two phases occurs via a spinodal decomposition of a homogeneous solid solution (Ti,Mo)(C,N) that is existent only at high temperatures (Fig. 7).

By means of MS analysis given in the previous section, pure TiN was observed to be very stable against vacuum up to 1500°C. However, TiN starts to react with WC (probably Mo_2C too) at about 1350°C, which results in N_2 elution. Moreover, such denitridation reactions are accelerated in the present of Co/Ni binders.

It is known that Mo and W do not form nitrides above 1000°C at normal N_2 pressure of 1 bar, and Mo_2C and WC are much more stable against N_2 than TiC and $\mathrm{Ti}(\mathrm{C}_{1-x}, \mathrm{N}_x)$. Nitrides tend to decompose under vacuum via evolution of nitrogen. On the other hand, carbides and carbonitrides react with nitrogen under formation of elemental carbon: $\langle \mathrm{TiC} \rangle + 1/2\mathrm{N}_2 \rightarrow \langle \mathrm{TiN} \rangle + \mathrm{C}$. The brackets $\langle\ \rangle$ are indicating that TiC and TiN are not separate phases but partners in a solid solution. In that case the three-phase equilibrium Ti(C,N), C and gas phase can be formulated in the usual way:

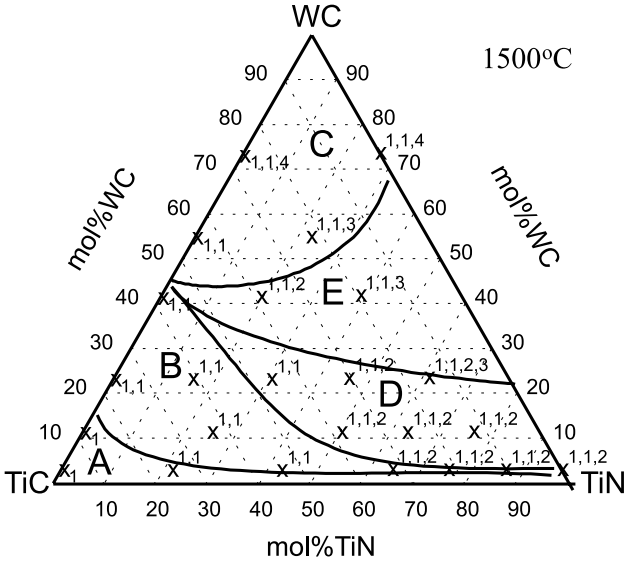

Fig. 6. Phase existence in the TiC–TiN–WC hard phase system. All samples were hot-pressed at 2300°C and then Ar-annealed at 1500°C for 168 h. The meanings of the numbers in the chart are: 1 – fcc phases of δ_1-$(\mathrm{Ti}_x, \mathrm{W}_{1-x})(\mathrm{C}_{x'}, \mathrm{N}_{1-x'})$ rich in Ti, and N and δ_2-$(\mathrm{Ti}_y, \mathrm{W}_{1-y}) \times (\mathrm{C}_{y'}, \mathrm{N}_{1-y'})$ rich in W and C; 2 – bcc W; 3 – hex W_2C ; and 4 – hex WC.

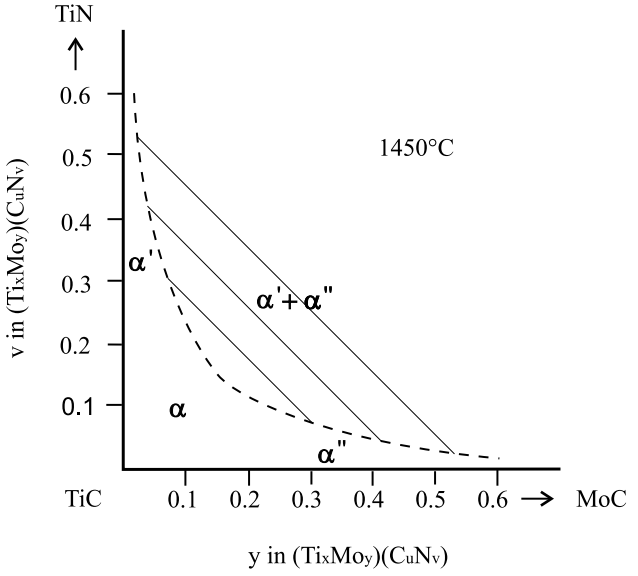

Fig. 7. Partial isothermal section of the TiC–TiN–"MoC" hard phase system at 1450°C, after [19].

$$\Delta G = -RT^* \ln K_p = -RT^* \ln \left[\frac{\left(a^*_{TiC} a_C\right)}{\left(a^*_{TiC} P^{1/2}_{N_2}\right)} \right].$$

Carbon as a phase has the activity $a_C = 1$ and if ideality of the solid solution is assumed, then $a_{TiN}/a_{TiC} = x_{TiN}/x_{TiC}$. By introducing the free energies of the formation of TiC and TiN, the equilibrium pressure P_{N_2} in equilibrium with graphite can be calculated for all temperatures and compositions of $Ti(C_x, N_{1-x})$ as illustrated in Fig. 8 [18].

Within the two-phase equilibrium:

$$Ti(C_x, N_{1-x})_z \rightarrow Ti(C_x, N_{1-x})_{z-\Delta z} + 1/2(1-x)\Delta z\ N_2,$$

the nitrogen partial pressure is a function both of x and z. In the presence of a liquid phase such as Ni or Co, the nitrogen partial pressure will of course influence the solubility of carbon (at carbon activity <1), nitrogen and titanium in the liquid binder metal, and consequently influence the metallurgical reactions. Thus, during the sintering of nitrogen-containing alloys, nitrogen pressure has to be adjusted within certain limits to the composition of the carbonitrides and the sintering temperature.

During sintering of cermets or cemented carbonitrides, as soon as the oxide film on the powder particles has been removed by the reductive processes, wetting by the binder metal melt sets in and the carbon-containing binder metal melt interacts with the hard phase particles. As could be demonstrated in investigations by Kieffer et al. [1], depending on the nitrogen pressure in the sintering atmosphere, carbon is able to displace nitrogen from the nitrides (at low nitrogen partial pressure) or nitrogen is able to displace carbon from the carbides. The nitrogen equilibrium pressure of titanium carbonitride in equilibrium with elementary carbon is, apart from the temperature, only determined by the composition of the carbonitride. If the carbon activity becomes <1, i.e., if the carbon supplier is a carbide e.g., Mo_2C or WC, the corresponding nitrogen equilibrium pressure is slightly reduced. Fig. 8 shows which nitrogen pressures are to be expected at least in the initial phases of the sintering process, i.e., when the carbon-containing liquid phase begins to react with the surface of the nitride or carbonitride particles. If the nitrogen partial pressure is considerably below the limits for quite a long time during sintering, it can be assumed that considerable amounts of titanium will be dissolved in the binder alloy. Therefore, the precipitation of intermetallic phases of the type Ni_3Ti might finally be the consequence [18].

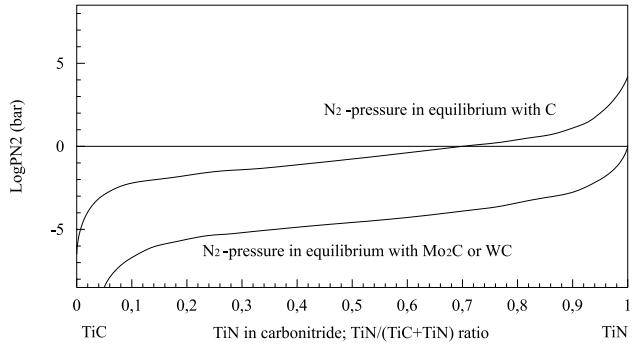

Fig. 8. Nitrogen equilibrium pressure of titanium carbonitride of different compositions at 1450°C, after [18].

The carbides of the IVth group metals and VC_{1-x} react readily with nitrogen under the formation of a carbonitride and graphite. The compositions of the carbonitrides are dependent on nitrogen pressure and temperature of the reaction. As predicted by thermodynamics, higher pressure of nitrogen leads to carbonitrides richer in nitrogen, at higher temperatures otherwise under identical conditions the nitrogen content in the carbonitrides becomes lower. NbC and Mo_2C react only to a very small extent with nitrogen, whereas TaC and WC appear to be stable against nitrogen even at very high pressures. Cr_3C_2 reacts with nitrogen of 300 bar under formation of a ternary compound $Cr_3(C, N)_2$ as reported by Kieffer and Ettmayer et al. [20].

3.6. Phase reactions

Yoshimura et al. [21] studied the phase reactions of a cermet with a composition of TiC–20%TiN–15%WC–10%TaC–9%Mo–5.5%Ni–11%Co by XRD measurements. The relative XRD intensities (I/I_0) and lattice parameters of each phase as functions of the sintering temperature are given in Fig. 9 again. The intensity (I/I_0) of TiC increases with increasing temperature, most remarkably in the range 1100–1200°C. In the meantime, the intensities (I/I_0) of Mo_2C, TaC, WC, and TiN decrease. Correspondingly, the lattice parameter of the TiC phase decreases, and the lattice parameter of the binder phase increases, respectively. This fact means that Mo_2C, TaC, WC, and TiN phases have considerably dissolved in TiC and binder phase. The Mo_2C phase dissolves most rapidly and completely disappears at 1200°C already. TaC and WC phases disappear at 1300°C. TiN dissolves more slowly in comparison with Mo_2C, TaC, and WC. A certain amount of TiN remains undissolved even at temperatures up to 1400°C. The dissolution of Mo_2C, TaC, WC, and TiN observed at temperatures below 1300°C must have taken place through solid-state diffusion, since liquid phase starts to appear first at approximately 1300°C.

On the cross-sections of "solid–liquid" reaction couples, four different zones were observed: (1) unreacted carbide compact; (2) diffusion zone where the liquid metal has penetrated along the grain boundaries; (3) reaction zone and (4) metal alloy zone where the metal

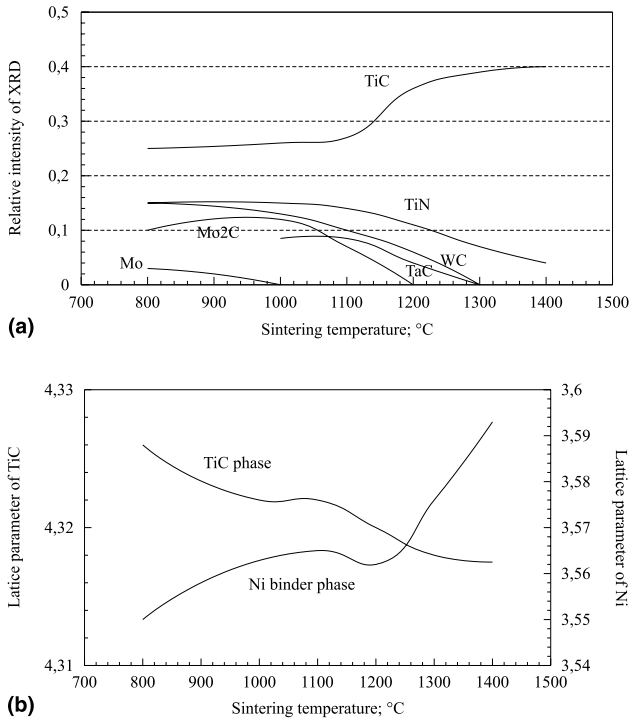

Fig. 9. (a) Relative intensities of XRD of Mo, Mo_2C, TaC, TiN and TiC vs. sintering temperature [21]. (b) Lattice parameters of TiC and Ni binder phase vs. sintering temperature [21].

melt has solidified and the carbide has re-precipitated from the melt. An example of such a cross-section is shown in Fig. 10. On one hand, Ti, Mo/W and C atoms dissolve from carbide compact into the Ni/Co melt. On the other hand, the Ni/Co metal melt penetrates into the carbide compact along the grain boundaries, which gives rise to penetration of liquid deep into the carbide compact and the formation of a reaction zone where melt

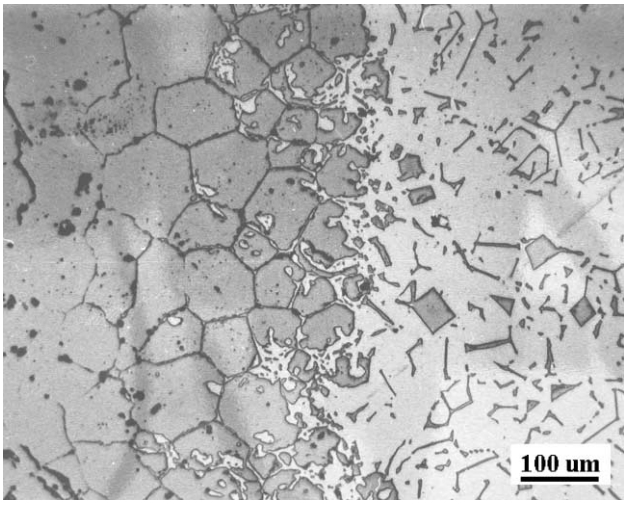

Fig. 10. Microstructure of the cross-section of $(Ti_{0.9}, Mo_{0.1})C$–Ni solid–liquid reaction couple.

and undissolved carbide particles coexist. Upon cooling down, dissolved Ti, Mo/W and C atoms re-precipitate in the form of mixed carbide in the Ni/Co melt region, and eventually the Ni/Co melt solidifies too. In the reaction zone, part of the compact carbides enters the solution of the Ni/Co melt and – on cooling – re-precipitates as mixed carbide, whereas part of the original carbide remains undissolved. The undissolved carbides in the reaction zones contain less Mo than the original carbides.

''Selective dissolution and selective re-precipitation'' of heavy elements during solid–liquid reactions were observed by SEM/EDS as shown in Fig. 11. They are probably the result of the fact that different carbides have quite different solubilities in the Co/Ni binder metals. The solubility of some metal carbides and nitrides in the binder metals is listed in Table 3 [22,23]. Due to the selective dissolution of Mo (or W) from the solid carbide compact, the melt contains relatively more Mo (W) than the carbide compact in equilibrium with it. Hence, the re-precipitating carbide must contain relatively more Mo (W) than the starting carbide compact in contact with the melt upon solidification (cooling down).

The interactions between hot-pressed $(Ti, W)(C, N)$ compacts and N_2 up to 30 bars have been studied for the entire compositional range of the TiC–TiN–WC system [13]. An example of the results is given in Fig. 12. Upon N_2 pressure, temperature and chemical composition, the quaternary $(Ti, W)(C, N)$ alloys may decompose into two fcc phases δ_1 and δ_2 and WC through: $(Ti, W)(C, N) + N_2 \rightarrow \delta_1 + \delta_2 + WC$, where $\delta_1 - (Ti_x, W_{1-x})(C_{x'}, N_{1-x'})$ is rich in Ti, and N and $\delta_2 - (Ti_y, W_{1-y})(C_{y'}, N_{1-y'})$ is rich in W and C (see Fig. 6). In the microstructure of an unattached area, $\delta_1 - (Ti_x, W_{1-x})(C_{x'}, N_{1-x'})$ is darker than $\delta_2 - (Ti_y, W_{1-y}) \times (C_{y'}, N_{1-y'})$ as shown in Fig. 12(a). The original (Ti,W)(C,N) grains near the surface were attacked by N_2 to form very fine structures where WC phase (white and very thin in shape) was observed. The element distributions across sample section show gradients of C, N and W (see Fig. 12(b)). N concentration decreases while C and W concentrations rise with increasing distance from the sample surface.

3.7. Mechanism of formation of ''core-rim'' structures in cermets

''Core-rim'' structure within the hard phases is the typical microstructure of cermets. As shown in Fig. 13, hard particles with ''bright core-dark rim'', or with ''bright rim-dark core'' can be observed. Some hard particles even have complex structure with an inner rim. Element analysis across the Ni binder phase and carbide grains was carried out by TEM/EDS. The compositions and preparation processes of TEM specimens are listed

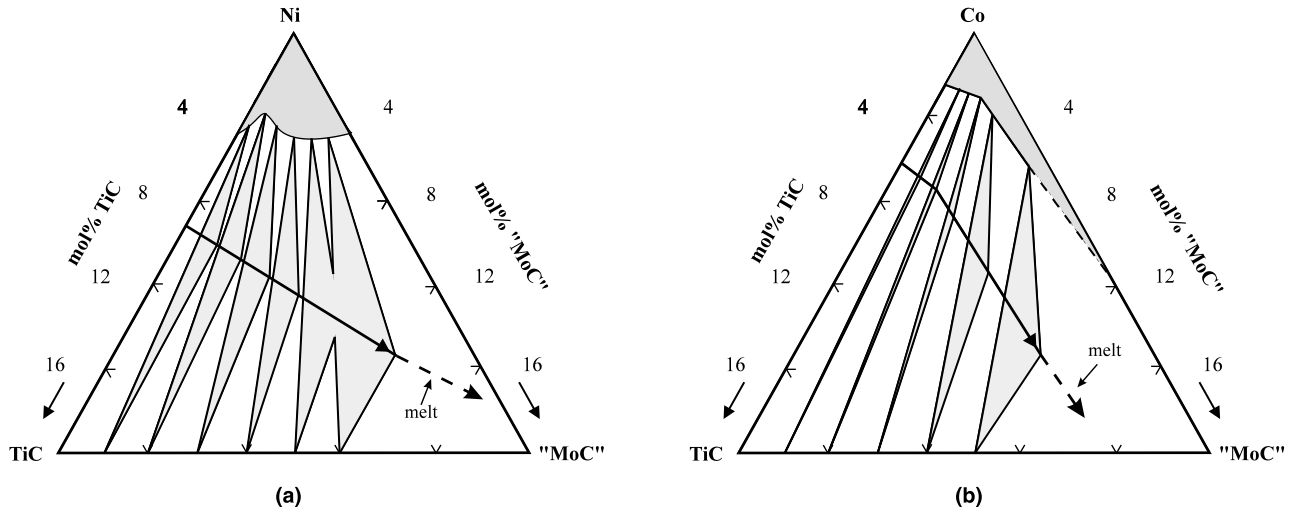

Fig. 11. Phase equilibria between melt, (Ti,Mo)C carbide and Ni/Co solid solution in solid/liquid reaction couples of: (a) Ni–(Ti,Mo)C near 1300°C and (b) Co–(Ti,Mo)C near 1350°C.

Table 3
Solubility of hard phases in liquid and solid metals [22,23]

Solubility of hard phases in liquid metals at 1400°C after [22]			Solubility of hard phase in solid binder metals at 1250°C after [23]		
Hard phase	in Ni (wt%)	in Co (wt%)	in Ni (wt%)	in Co (wt%)	in Fe (wt%)
TiC	11	10	1	5	<0.5
TiN	<0.5	<0.5	<0.1	<0.1	<0.1
Mo_2C	36	39	13	8	5
WC	27	39	22	12	7
TaC	6.3	6.3	3	5	0.5
NbC	7.0	8.5	5	3	1
VC	14	19	–	–	–
Cr_3C_2	–	–	12	12	8

in Table 4. Fig. 14 gives a photograph of sample 6N. The white particles are hard phase and the gray areas are Ni binder phase. The dark spots in the microstructure are the points where chemical compositions were analyzed by TEM/EDS. Mo-rich rims are clearly demonstrated in Fig. 15.

Ti, Mo concentrations in the Ni binder phase are probably controlled by the stoichiometry factor z as well as by the nitrogen content of the hard phase $(Ti,Mo)(C,N)_z$. Decreasing of the stoichiometry factor z will improve the solubility of Ti and Mo, while increasing of nitrogen content in the hard particles will decrease the Ti concentration but largely increase the Mo concentration. Sample TM8102 has a stoichiometric carbide $(Ti_{0.8}, Mo_{0.2})C$, P4 has a sub-stoichiometric carbide $(Ti_{0.8}, Mo_{0.2})C_{0.9}$, while 6N has a slightly sub-stoichiometric carbonitride phase $(Ti_{0.8}, Mo_{0.2})(C_{0.7}, N_{0.3})_{0.97}$. As shown in Fig. 16, the Ti, Mo concentrations and the total amount (Ti + Mo) in the Ni solid solution of sample P4 are nearly double that of TM8102. Sample 6N has a much higher Mo content and a lower Ti content than those of both P4 and TM8102. The total amount of (Ti + Mo) in the binder phase of 6N is similar to that of P4, whereas higher than that of TM8102.

We can assume that quasi-isothermal conditions will prevail and in the ideal case of equilibration during sintering. We will end up with a binder melt somewhat higher in Mo (or W if WC is present, the same for the follows) than the carbides in equilibrium with the melt. In reality, we will have non-equilibrium conditions because the diffusivities in the carbide phase are lower by several orders of magnitude than the diffusivities in the liquid phase. Furthermore, the rates of dissolution will depend on the grain sizes of the carbide particles. During liquid phase sintering of a cermet alloy, it can be anticipated that in the first few minutes of liquid phase formation, the small particles of (Ti,Mo)C will go into solution at a higher rate than the larger particles. Since this constitutes a non-equilibrium condition (the melt has the same Ti/(Ti + Mo) atom ratio as the carbide phase), a Mo depleted (Ti,Mo)C will start

(a) SEM back scatter images

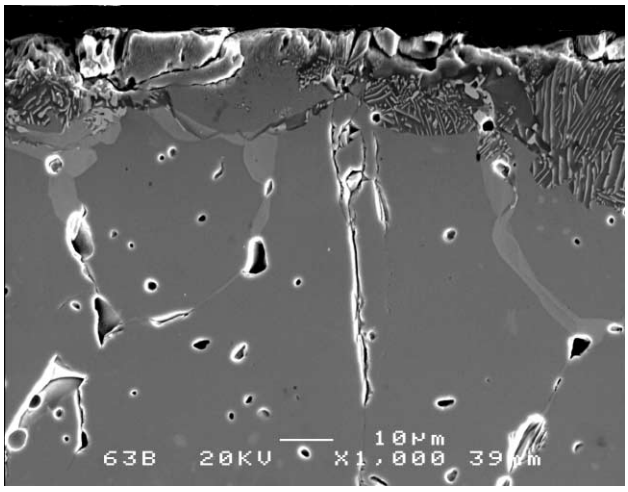

(b) EPMA measurement

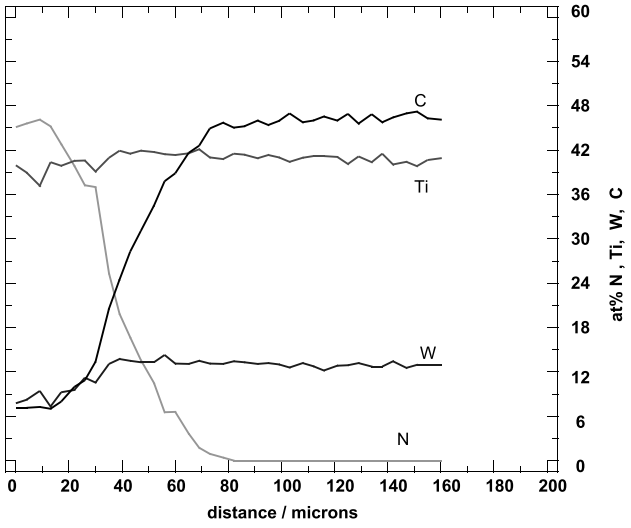

Fig. 12. (a) SEM microstructure and (b) element distribution of the surface interaction zone of a hot-pressed (Ti,W)(C,N) sample after N_2 annealing at 1500°C and 30 bar N_2 (WC/TiC/TiN = 24/76/0 in mol%).

to re-precipitate, probably epitaxially, on some favorable lattice sites of undissolved larger (Ti,Mo)C particles. Because of this re-precipitation, some more (Ti,Mo)C particles will go into solution and some more Mo-depleted (Ti,Mo)C particles will precipitate. If this Mo-depleted (Ti,Mo)C phase on re-precipitation completely surrounds a large original (Ti,Mo)C particle and seals it off from the action of the liquid phase, we will end up with a "bright core – dark rim" microstructure. If, on the other hand, the re-precipitated Mo-depleted (Ti,Mo)C nucleates only on one favorable nucleation site of an original (Ti,Mo)C particle, the original particle will gradually be eaten away by the liquid. Only during the cooling-down period the Mo-rich liquid will form a Mo-rich (Ti,Mo)C rim (bright) around the Mo-depleted core ("dark core – bright rim"

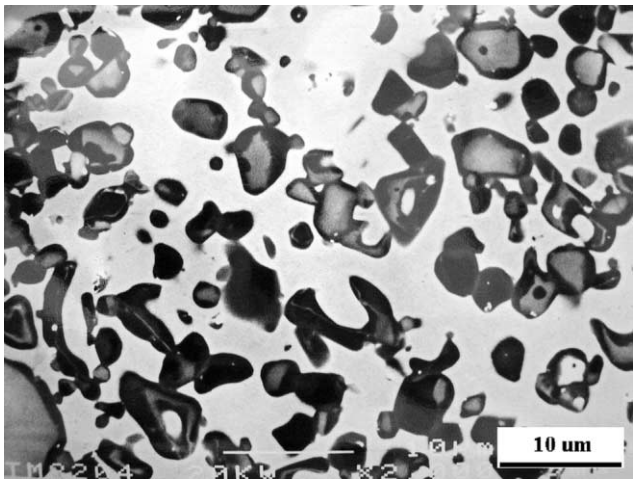

Fig. 13. "Core-rim" structure in sample TM8102 observed by SEM back scatter image.

microstructure). By such a mechanism, the simultaneous occurrence of the two types of hard particles with bright cores and dark rims or with bright rims and dark cores might be explained. Furthermore, it is highly doubtful whether any supplier of pre-alloyed carbide material will really be able to provide a completely homogeneous pre-material without *any* compositional gradients. Inhomogeneous pre-materials obviously will lead to somewhat inhomogeneous microstructural features.

3.8. Phase observation and grain size

The microstructure of cermets and cemented carbonitrides is determined by the compositions of their hard phases in the WC–TiC–TiN and WC–TiCN–TaC systems (see Figs. 2(e) and (f)). If the hard phase composition of an alloy is located in the cermet compositional range of (Ti,W)(C,N) + Co/Ni, WC phase will not be observed. On the other side, WC phase will be observed in the cemented carbonitride range of WC + (Ti,W)(C,N) + Co/Ni. In fact, the existence of WC phase in the microstructure is the result that WC has a maximum solubility in the cubic phases of (Ti,Ta)(C,N). The solubility of WC in TiC and TaC is about 40 and 10 mol%, respectively (see Figs. 2(e)–(f) and Fig. 6). Fig. 17 gives a micrograph of a sample with hard phase composition of WC/TiC = 42/58 (in mol%). The microstructure is composed of faceted WC with large elongated grains and a spherical "core-rim type" (Ti,W)C with a Ti-rich core. Because almost all WC has dissolved into TiC, only a few undissolved WC grains were observed in the microstructure.

As for nitrogen-containing cemented carbonitrides and cermets, TiN usually acts as a grain growth inhibitor and produces very fine-grained microstructures with

Table 4
Compositions and preparing process of TEM specimens

Samples	Chemical compositions	Starting materials	Preparing process
TM8102	$(Ti_{0.8}, Mo_{0.2})C + 50$ vol% Ni	$(Ti_{0.8}, Mo_{0.2})C$; Ni	Vacuum sintered; 1 h 1400°C, 8×10^{-2} mbar
P4	$(Ti_{0.8}, Mo_{0.2})C_{0.9} + 18$ mol% Ni	TiC, Mo_2C, C, Ni	Vacuum sintered; 1 h 1500°C, $10 \sim 20$ mbar
6N	$(Ti_{0.8}, Mo_{0.2})(C_{0.7}, N_{0.3})_{0.97} + 18$ mol% Ni	$(Ti_{0.8}, Mo_{0.2})(C_{0.7}, N_{0.3})_{0.97}$, Ni	Vacuum sintered; 1 h 1500°C, 80 mbar N_2

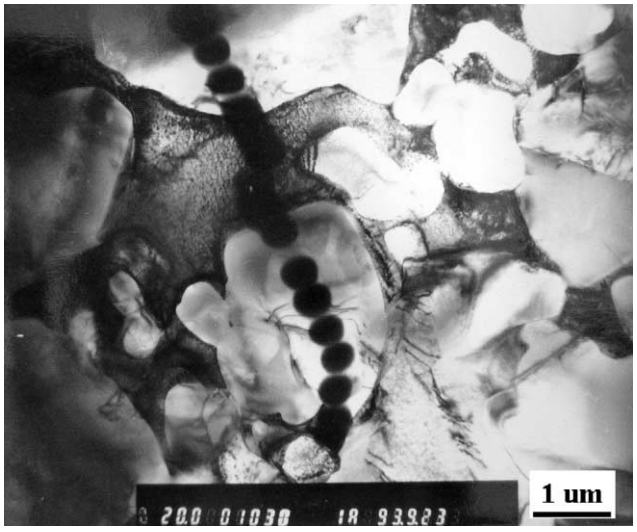

Fig. 14. TEM image of sample 6N with EDS analysis spots (dark).

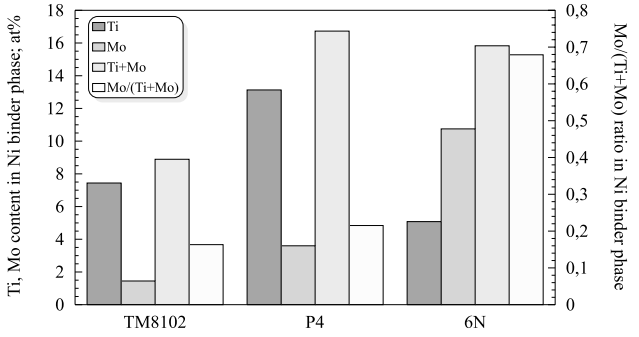

Fig. 16. Binder phase compositions of TM8102, P4 and 6N measured by TEM/EDS.

spherical WC-rich grains. Generally, the grain size of the hard phases decreases with increasing N/(C + N) content of the alloy. Upon increase of the TiN content, the WC-rich (or pure WC) grain becomes much less faceted. The (Ti,W)(C,N) phase also has a ''core-rim'' type structure though the individual grains can hardly be seen at low magnification. Moreover, the WC phase content in the microstructure increases if the N/(C + N) ratio of the alloys increases. An example of the microstructure of a N-containing alloys is given in Fig. 18.

3.9. Functionally graded cemented carbonitrides

Different types of functionally graded cemented carbonitrides (FGCC) have been prepared through direct

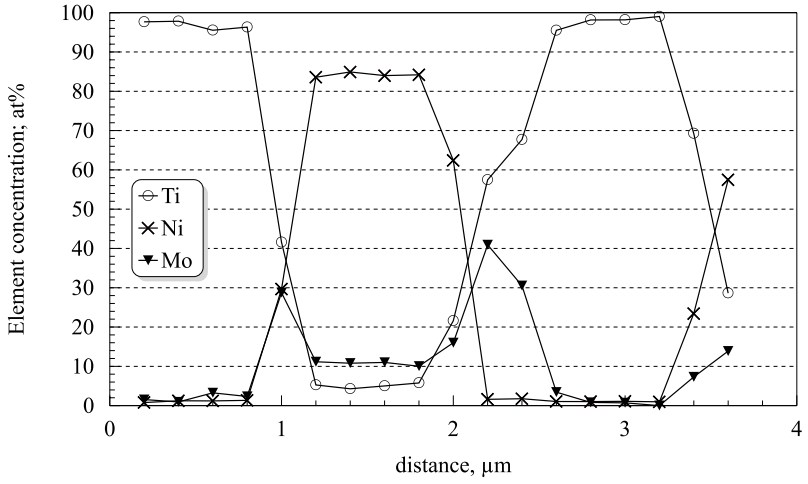

Fig. 15. Element distribution across grains of 6N specimen measured by TEM/EDS.

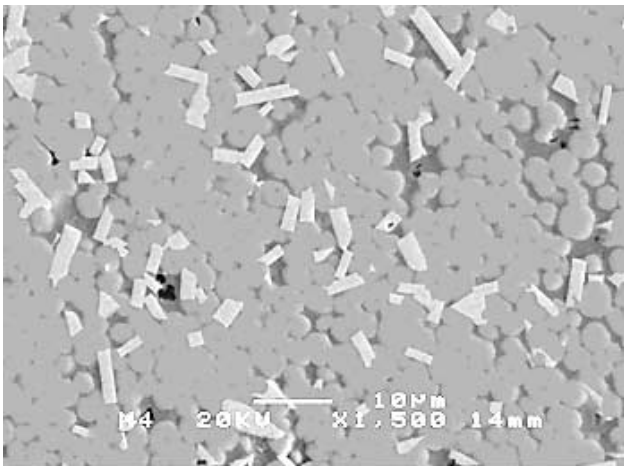

Fig. 17. SEM image of an alloy sample (WC/TiC = 42/58 in mol%; without nitrogen). Coarse-grained microstructure with faceted bright WC grains.

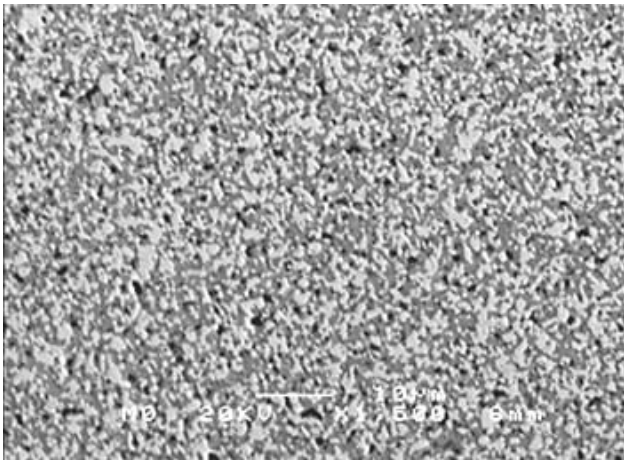

Fig. 18. SEM image of an alloy sample (WC/TiC/TiN = 55/25/20 in mol%). Fine-grained structure of both the WC-rich and TiC-rich phase.

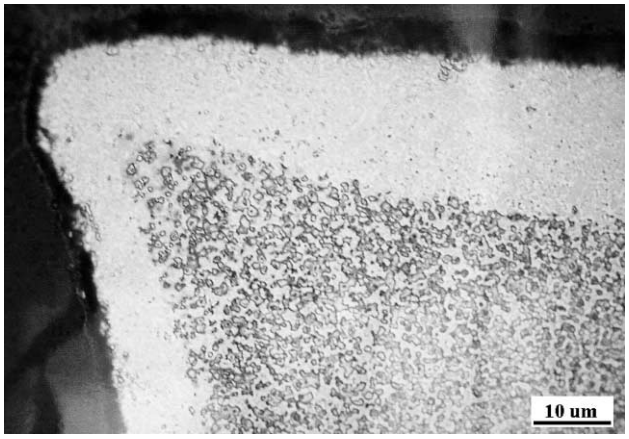

(a)

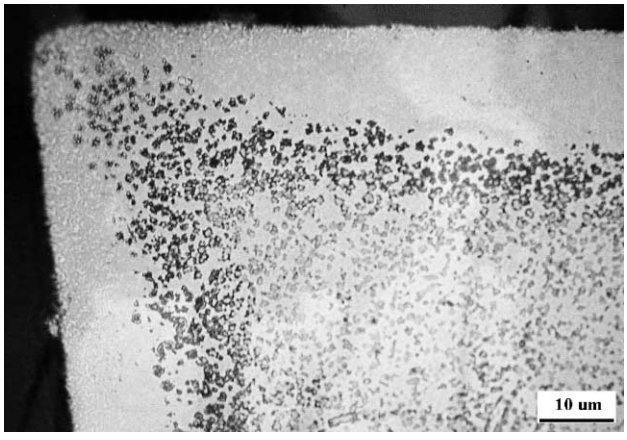

(b)

Fig. 19. Microstructures of cross-sections of some cemented carbonitrides: (a) entire CFL surface layer; (b) CFL surface layer with cubic phase enriched cutting edge.

sintering by careful alloy design and process (especially atmosphere) control [12–16]. Some examples of the FGCC microstructures are given in Figs. 19–21.

Fig. 19(a) shows a typical CFL layer covering the entire surface of the insert. By modifying the sintering atmosphere, CFL substrate with more cubic phase enrichment in the cutting edge can be prepared (see Fig. 19(b)). The composition of the starting materials can be either nitrogen-containing (Ti,W)(C,N) + Co/Ni green compacts, or non-nitrogen-containing (Ti,W)C + Co/Ni green compacts with nitrogen pre-treatment [12–14].

Another type of FGCC material features a cubic phase-rich, WC phase-free cermet surface layer which has compositional gradients of Ti, W, Co, C and N up to 500 μm, depending on the overall composition of the alloy. Fig. 20(a) gives an example of the microstructure of such FGCC material with high wear-resistant cermet surface, high tough cemented carbonitride substrate. Gradation of chemical composition was observed in the surface layer as shown in Fig. 20(b) measured by GDS. The experimental details of GDS measurement are given in [12,13]. The depth of the compositional gradient of this alloy is about 30 μm.

Even multi-layered FGCC insert materials can be fabricated by direct sintering. As shown in Fig. 21, the as-sintered material consists of a TiCN high wear-resistant outermost surface, a CFL underneath WC + Co tough intermediate layer and cemented carbonitride strong core. Materials with similar surface modification must be prepared by costly CVD or PVD [6] before direct sintering technology developed in this work. Because of the graded structures within each layer as shown in Fig. 21(b), this new type of insert material is believed even to outperform the state-of-the-art coated cemented carbides.

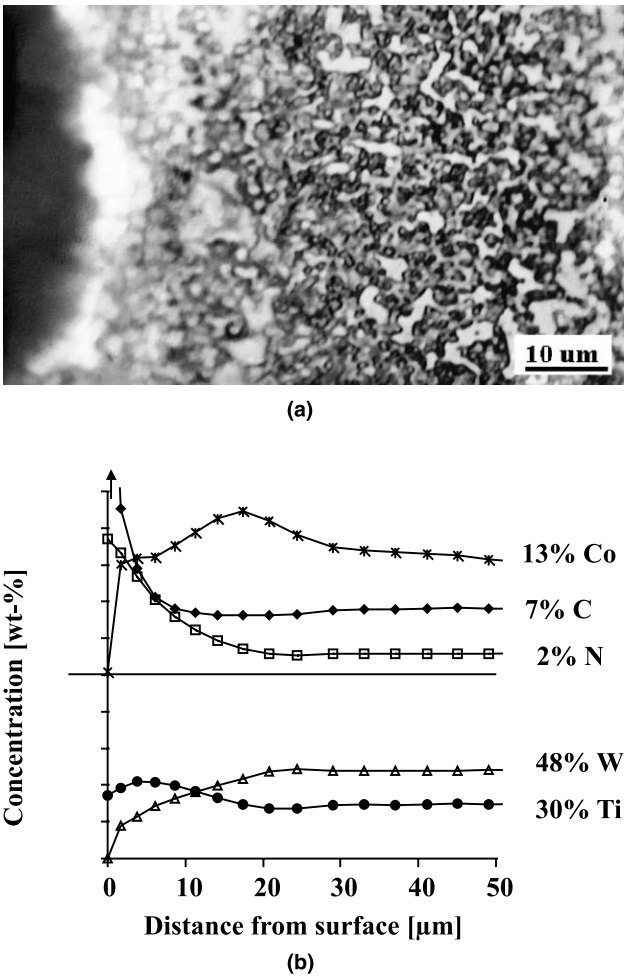

Fig. 20. FGM cermet surface layer on a cemented carbonitride substrate: (a) microstructure of the cross-section and (b) GDS composition depth analysis.

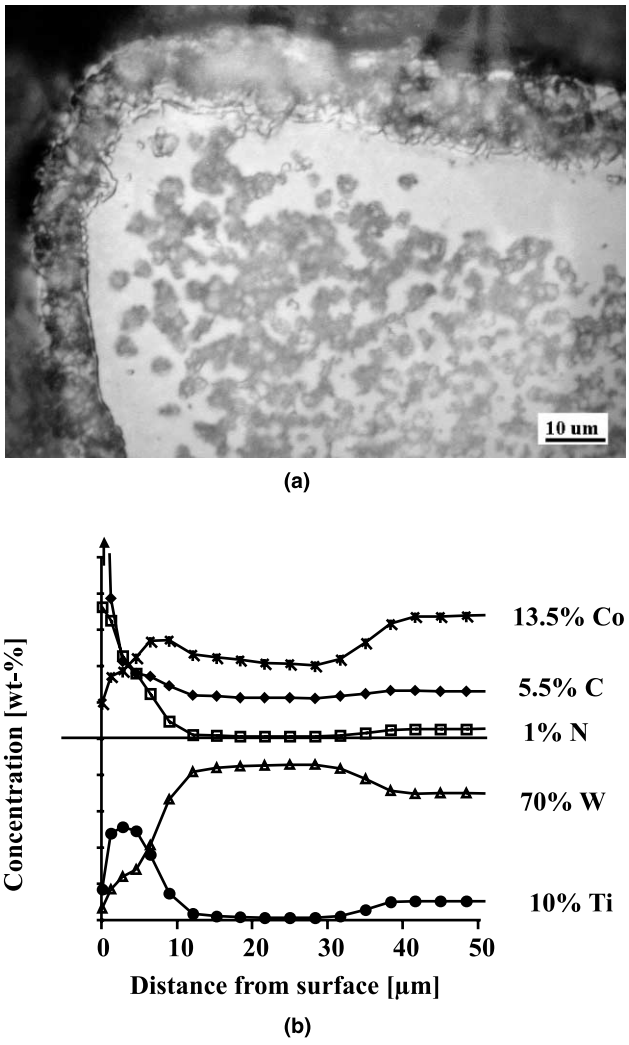

Fig. 21. Microstructure of a cemented carbonitride with multi-layered FGM surface: (a) microstructure of the cross-section and (b) GDS composition depth analysis.

4. Conclusions

- Melting behaviors of cermet and cemented carbonitride alloys have been studied by DTA and DSC. Regardless of their Ti/W ratios and C/N ratios, the WC + (Ti,W)(C,N) + Co cemented carbonitrides have a constant melting point temperature of 1350°C. (Ti,W)(C,N) + Co cermets have melting point temperatures in the range 1350–1450°C, depending on the Ti/W and C/N ratios of the alloy. The addition of TaC/NbC has basically no influence on the melting points of the alloys.
- During liquid phase sintering, particle re-arrangement of all (Ti,W)(C,N) + Co cermets and WC + (Ti,W)(C,N) + Co cemented carbonitrides starts at about 1300°C. Liquid phase sintering was observed by DIL at 1350°C and 1400–1450°C for cemented carbonitrides and cermets, respectively.
- Gas evolution was investigated by MS. Oxide films on the surface of particles are almost completely reduced below 1300°C. Outgassing process terminates at 1300°C as soon as particle re-arrangement begins.
- TiN is very stable against vacuum up to at least 1500°C. In the presence of carbon source such as WC, Mo_2C and graphite, denitridation will be detected. The denitridation is acerbated through Co/Ni binder metals due to enhanced diffusion through binder metals.
- Thermodynamic stability of hard phases, phase reactions and phase equilibria within WC–TiC–TiN system have been entirely studied.
- Insert materials with different FGCC modifications have been successfully prepared by direct sintering. As-sintered FGCC inserts are believed to compete or even outperform traditional coated carbides due to their unique graded surface structure.

Acknowledgements

Widia GmbH and Dr. van den Berg, the general manager of R&D department of Widia GmbH are gratefully acknowledged for the financial support of the FGCC project. Austrian Academic Exchange Service (OEAD) is thanked by Dr. Limin Chen for the scholarship within the framework of the ''North-South-Dialogue Programme'' which made it possible for him to complete his Ph.D. dissertation work at the Vienna University of Technology during the period 1992–1995. Dr. Chen would like to give his special thanks to Dr. Kny, the director of the Division of Materials Technology of ARCS, who gave him the opportunity to work at the Austrian Research Center Seibersdorf (ARCS) as well as the support to the project. Thanks are also due to Dr. Sejc, Dipl–Ing. Garcia and Mr. Kral of TU Vienna, Ing. Kladler and Ing. Trampert of the ARCS, for their contribution to some of the experiments. Dr. Chen would also like to thank Mr. Cippel of SinterMet, Inc. and his wife Dr. Hua Ge, for their assistance during the preparation of the manuscript.

References

[1] Kieffer R, Ettmayer P, Freudhofmeier M. About nitrides and carbonitrides and nitride-based cemented hard alloys. In: Hausner H, editor. Modern development in powder metallurgy, vol. 5, 1971. p. 201–14.

[2] Ettmayer P, Lengauer W. The story of cermets. Powder Metall Int 1989;21(2):37–8.

[3] Pastor H. Titanium carbonitride based hard alloys for cutting tools. Mater Sci Eng A 1988;105/106:401–9.

[4] Ettmayer P, Kolaska H, Lengauer W, Dreyer K. Ti(C,N) cermets metallurgy and properties. Int J Refract Met & Hard Meter 1995;13:343.

[5] Doi H. Advanced TiC and TiC–TiN based cermets. In: Proceedings of the Second International Conference Science of Hard Materials, 1986. p. 489–523.

[6] van den Berg H, Konig U, Sottke V, Tabersky R, Westphal H. Die bedeutung von modifizierten randzonen fur die hartmetallbeschichtung. In: Ruthardt R, editor. Hartstoffe, Hartstoffschichten, Werkzeuge, Verschleisssschutz of Pulvermetallurgie in Wissenschaft und Praxis Band 13. Werkstoff-Informationsgesellschaft mbH; 1997. p. 77–87.

[7] Suzuki H, Hayashi K, Taniguchi Y. The β-free layer near the surface of vacuum-sintered WC–β-Co alloys containing nitrogen. Trans Jpn Inst Met 1981;22(11):758–64.

[8] Yohe WC. The development of cubic-carbide-free surface layers in cemented carbides without nitrogen. In: Bildstein H, Eck R, editors. Proceedings of the 13th International Plansee Seminar. Metallwerk Plansee, vol. 2, 1993. p. 151–68.

[9] Schwarzkopf M, Exner HE, Fischmeister HF. Kinetics of compositional modification of (W,Ti)C–WC–Co alloy surfaces. Mater Sci Eng A 1988;105/106:225–31.

[10] Hayashi K, Suzuki H, Doi Y. Effect of β-free layer of substrate on properties of cemented carbide coated with TiC by CVD process. J Jpn Soc Powder and Powder Metall 1985;32(7):28–31.

[11] Tsuda K, Ikegaya A, Isobe K, Kitagawa N, Nomura T. Development of functionally graded sintered hard materials. Powder Metall 1996;39(4):296–300.

[12] Chen L, Lengauer W. Metallurgical mechanisms and processing technologies of FGM (Ti,W)(C,N)-Co hardmetals. Internal Reports of Austrian Research Center, OEFZS-A – 4185, 1997.

[13] Chen L, Lengauer W. Metallurgical mechanisms and processing technologies of FGM (Ti,W)(C,N)-Co hardmetals. Internal Reports of Austrian Research Center, OEFZS-A – 4516, 1998.

[14] Chen, L, Lengauer W, Dreyer K. Advances in modern nitrogen-containing hardmetals and cermets. In: Proceedings of the European Conference on Advances in Hard Materials, 8–10 November 1999; Production sponsored by EHMG & EPMA, Turin, Italy. p. 463–73.

[15] Lengauer W, Chen L, Garcia J, Ucakar V, Dreyer K, Kassel D, Daub HW. Diffusion–controlled surface modification of functionally-gradient (Ti,W)C-based cemented carbonitrides. In: Proceedings of the 1999 International Conference on Powder Metallurgy & Particulate Materials sponsored by the Metal Powder Industries Federation and APMI International, vol. 3, Part 10, 20–24 June 1999; Vancouver, BC, Canada. p. 85–96.

[16] Chen L, Lengauer W, Daub HW, Dreyer K, Kassel D. German Patent DE 198 45 376 A1, 13 January 2000.

[17] Dreyer K, Daub W, Holzhauer H, Orths S, Kassel D, Rodiger K. Trends in der Hartmetallfertigung: Legierungen, Verfahren, Produkte. In: Ruthardt R, editor. Hartstoffe, Hartstoffschichten, Werkzeuge, Verschleisssschutz of Pulvermetallurgie in Wissenschaft und Praxis Band 13. Werkstoff-Informationsgesellschaft mbH; 1997. p. 3–27.

[18] Ettmayer P, Kolaska H, Dreyer K. Effect of the sintering atmosphere on the properties of cermets. Powder Metall Int 1991;23(4):224–9.

[19] Rudy E. Boundary phase stability and critical phenomena in higher order solid solution systems. J Less-Common Met 1973;3:343–70.

[20] Kieffer R, Ettmayer P. Grundlagen und Neuentwicklungen auf dem Gebiet metallischer und nichtmetallischer Hartstoffe. Chemie-Ing.-Tech. 42 Jahrg./Nr.9/10 1970:589–99.

[21] Yoshimura H, Sugizawa T, Nishigaki K, Doi H. Reaction occurring during sintering and the characteristics of TiC–20TiN–15WC–10TaC–9Mo–5.5Ni–11Co cermets. R & HMDecember 1983:170–74.

[22] Ettmayer P, Kolaska H, Lengauer W, Dreyer K. Cermetlegierungen-Metallurgie und Eigenschaften. In: Proceedings of the 13th International Plansee Seminar'93, HM2, vol. 4, 24–28 May 1993; Tirol, Austria. p. 191–208.

[23] Edwards R, Raine T. The solid solubility of some stable carbides in cobalt, nickel and iron at 1250°C. In: Proceedings of the First International Plansee Seminar, 1952. p. 232.